Silica-Supported PdGa Nanoparticles

Metal Synergy for Highly Active and Selective CO_2-to-CH_3OH Hydrogenation

Docherty, Scott R.; Phongprueksathat, Nat; Lam, Erwin; Noh, Gina; Safonova, Olga V.; Urakawa, Atsushi; Copéret, Christophe

DOI
10.1021/jacsau.1c00021

Publication date
2021

Document Version
Final published version

Published in
Journal of the American Chemical Society

JACS Au
AN OPEN ACCESS JOURNAL OF THE AMERICAN CHEMICAL SOCIETY

pubs.acs.org/jacsau

Article

Silica-Supported PdGa Nanoparticles: Metal Synergy for Highly Active and Selective CO_2-to-CH_3OH Hydrogenation

Scott R. Docherty, Nat Phongprueksathat, Erwin Lam, Gina Noh, Olga V. Safonova, Atsushi Urakawa, and Christophe Copéret*

Cite This: *JACS Au* 2021, 1, 450–458

Read Online

ACCESS | Metrics & More | Article Recommendations | Supporting Information

ABSTRACT: The direct conversion of CO_2 to CH_3OH represents an appealing strategy for the mitigation of anthropogenic CO_2 emissions. Here, we report that small, narrowly distributed alloyed PdGa nanoparticles, prepared via surface organometallic chemistry from silica-supported Ga^{III} isolated sites, selectively catalyze the hydrogenation of CO_2 to CH_3OH. At 230 °C and 25 bar, high activity (22.3 mol_{MeOH} mol_{Pd}^{-1} h^{-1}) and selectivity for CH_3OH/DME (81%) are observed, while the corresponding silica-supported Pd nanoparticles show low activity and selectivity. X-ray absorption spectroscopy (XAS), IR, NMR, and scanning transmission electron microscopy–energy-dispersive X-ray provide evidence for alloying in the as-synthesized material. In situ XAS reveals that there is a dynamic dealloying/realloying process, through Ga redox, while operando diffuse reflectance infrared Fourier transform spectroscopy demonstrates that, while both methoxy and formate species are observed in reaction conditions, the relative concentrations are inversely proportional, as the chemical potential of the gas phase is modulated. High CH_3OH selectivities, across a broad range of conversions, are observed, showing that CO formation is suppressed for this catalyst, in contrast to reported Pd catalysts.

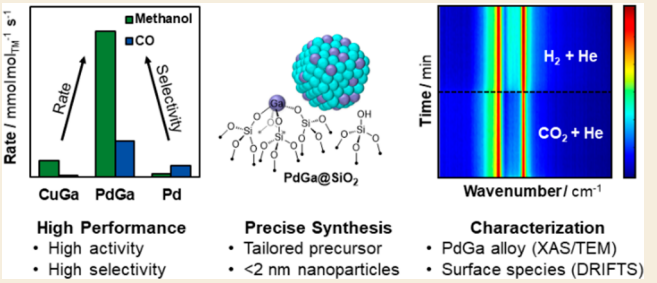

KEYWORDS: *CO_2 hydrogenation, Heterogeneous catalysis, Alloys, Nanoparticles, Operando spectroscopy, Hydrogenation*

INTRODUCTION

The conversion of CO_2 to liquid fuels has garnered significant attention in recent years, as a strategy to mitigate anthropogenic CO_2 emissions and an alternative source of platform chemicals to fossil fuels.[1] In particular, the direct hydrogenation of CO_2 to CH_3OH (eq 1–Scheme 1a) has been highlighted as an appealing target.[2−5] For this purpose, metallic nanoparticles supported on oxide supports, modified with various promoters, have been extensively studied. For the most part, efforts have focused on copper particles combined with zinc oxide/alumina ($Cu/ZnO/Al_2O_3$)[6−8] or supported on zirconia (Cu/ZrO_2).[5,9−11] However, these Cu-based catalysts show limited activity, decreasing selectivity with increasing conversion, and suffer from deactivation.[12] Therefore, alternative metals, oxide promoters, and supports have been investigated.[5] In this context, Pd-containing systems (Pd/MO_x)[13−18] show superior activities to those based on Cu in the hydrogenation of CO_2 to CH_3OH when supported on reducible oxides (ZnO or Ga_2O_3). In particular, Pd–Ga-based systems have attracted attention in recent years, as highly active catalysts for the hydrogenation of CO_2 to methanol.[13,14,19−23] These systems, based on Pd/Ga_2O_3, Pd–Ga/SiO_2, $Pd/Ga_2O_3/SiO_2$, or PdGa colloidal nanocrystals, often show superior activity when compared to Cu-based catalysts. However, Pd-based catalysts display low CH_3OH selectivity

Scheme 1. (a) Thermodynamics of CO_2 Hydrogenation. (b) Comparison of Reported Pd/Ga Systems and This Work

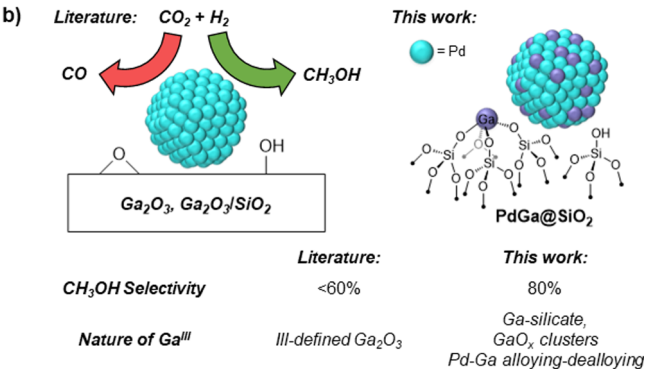

Received: January 18, 2021
Published: March 17, 2021

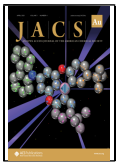

Table 1. Physicochemical Properties of Reduced Materials

material	EA,wt %	particle size,[a] nm	CO chemisorption,[b] $mol_{CO}\ mol_{Pd}^{-1}$ (D_{CO})	H_2 chemisorption, $mol_{H2}\ mol_{Pd}^{-1}$	H/CO ratio	terminal CO stretch, cm^{-1}	bridging CO stretch, cm^{-1}
$PdGa@SiO_2$	Pd: 1.08 Ga: 1.66	1.6 ± 0.4	0.55 (55%)	0.56	2.0	2086	1960
$Pd@SiO_2$	Pd: 1.61	1.6 ± 0.3	0.61 (61%)	0.91	3.0	2094	1967

[a]Particle size determined by TEM. [b]Dispersion assumes 1:1 ratio $CO/Pd_{surface}$.

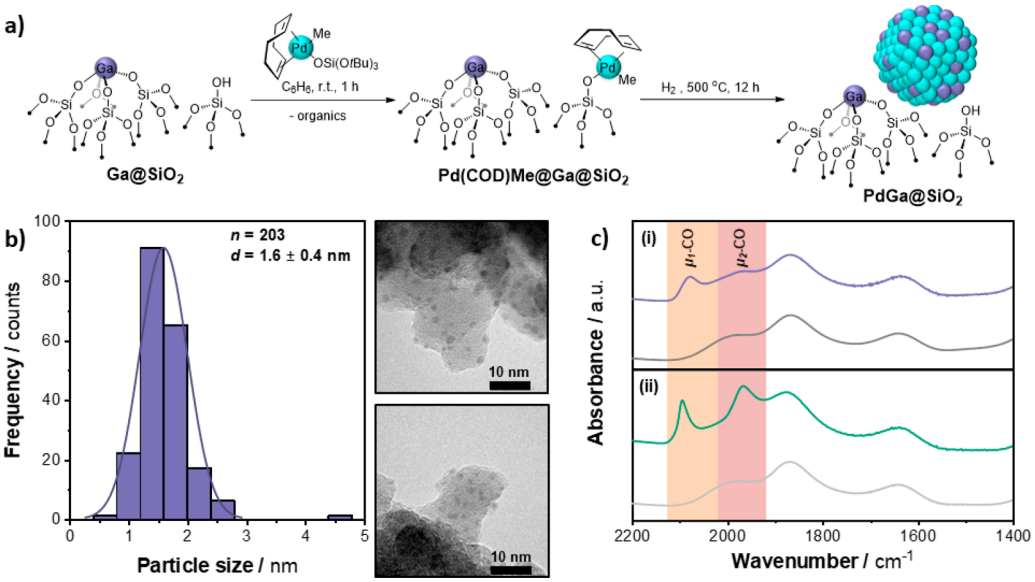

Figure 1. (a) Synthetic procedure for $PdGa@SiO_2$. (b) Particle size distribution and representative TEM images for $PdGa@SiO_2$; and (c) CO-adsorption IR for (i) $PdGa@SiO_2$ exposed (purple, top) and prior to CO adsorption (gray, bottom); (ii) $Pd@SiO_2$ exposed (green, top) and prior to CO adsorption (gray, bottom). 10 mbar CO.

(<60%, Scheme 1b) due to the competing reverse water gas shift (RWGS) reaction (eq 2).[13,21] As such, molecular insights into the origin of the high activity of these systems as well as the underlying cause of the undesired RWGS reaction is critical to the design of improved CO_2 hydrogenation catalysts.

Our group has recently shown that surface organometallic chemistry (SOMC) can be an ideal approach to control metal−support interfaces and to improve the catalytic performance for various reactions including CO_2 hydrogenation.[24−28] We thus reasoned that SOMC could provide a tool to tune the CO_2 hydrogenation activity and selectivity of Pd by tailoring the interface between Pd and Ga. Herein, we report the synthesis of a bimetallic PdGa system, consisting of small PdGa alloy nanoparticles generated by grafting a tailored Pd molecular precursor, $Pd(COD)Me(OSi(O^tBu)_3)$ (**1**) (COD = 1,5-cyclooctadiene), on the silanol sites of silica-containing isolated Ga^{III} sites ($Ga@SiO_2$),[29] followed by reduction under H_2. This material ($PdGa@SiO_2$, Scheme 1b), characterized by transmission electron microscopy (TEM), chemisorption, X-ray absorption spectroscopy (XAS), energy-dispersive X-ray (EDX) mapping as well as CO-adsorption infrared (IR) spectroscopy, shows high activity and unprecedented selectivity in the hydrogenation of CO_2 to CH_3OH when compared to reported Pd-containing catalysts and conventional Cu-based systems. The PdGa nanoparticles undergo partial dealloying under CO_2 hydrogenation as confirmed by XAS, but Pd remains metallic throughout the reaction, and Ga is partially oxidized but remains highly dispersed. The absence of large domains of Ga_2O_3, which are known to promote the RWGS (forming CO), probably explains the high methanol selectivity.[30] An analysis of strongly bound surface adsorbates by nuclear magnetic resonance (NMR) spectroscopy and IR suggests the presence of mostly methoxy moieties. Transient operando diffuse reflectance infrared Fourier transform spectroscopy (DRIFTS) and multivariate curve resolution (MCR) analyses show that methoxy and carbonyl species are preferentially stabilized under CO_2-rich conditions, while formate moieties are only detected under H_2-rich conditions. These observations parallel the alloying−dealloying of PdGa, indicating that the catalyst is highly dynamic, with implications for its reactivity and selectivity in CO_2 hydrogenation.

RESULTS AND DISCUSSION

Synthesis and Characterization of Supported Materials

We first developed a tailored Pd precursor that is amenable to grafting on silica and nanoparticle formation while releasing all its organic ligands: $Pd(COD)Me(OSi(OtBu)_3)$, **1** (Supporting Information S2 and S3). We first evaluated the grafting of **1** on silica dehydroxylated at 700 °C (SiO_{2-700}, 0.26 mmol − OH g^{-1}) that affords a monografted complex, (≡SiO)Pd(COD)-Me, with a concomitant liberation of 0.8 equiv of $HOSi(OtBu)_3$ per Pd (Supporting Information S4). An IR analysis of the grafted material (Supporting Information S5) reveals the emergence of C−H stretching (3100−2700 cm^{-1}) and bending (1700−1300 cm^{-1}) bands, alongside a decreased intensity for the isolated ≡SiOH band at 3747 cm^{-1}, indicative of grafting through silanol groups. ^{13}C cross-polarization magic-angle spinning (CP-MAS) NMR (Support-

https://doi.org/10.1021/jacsau.1c00021
JACS Au 2021, 1, 450−458

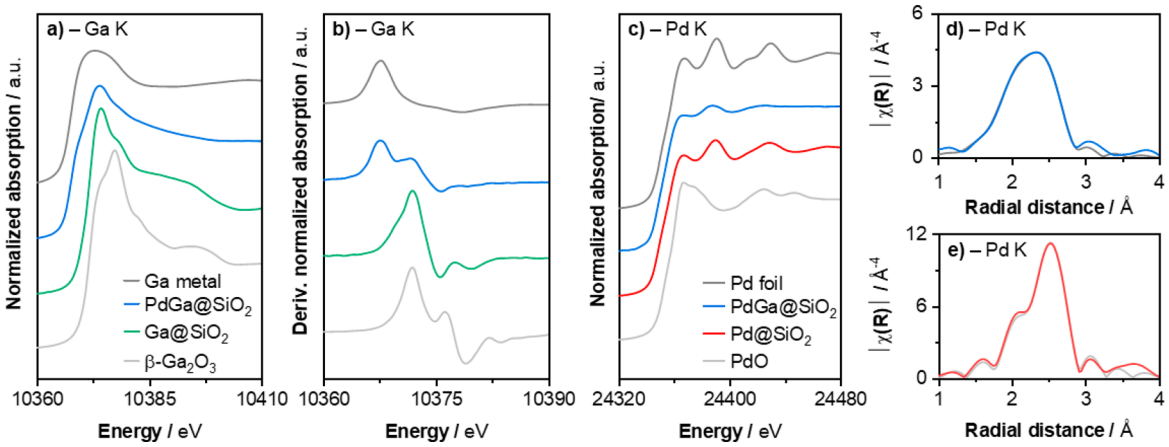

Figure 2. Normalized XANES spectra for (a) Ga K edge, (b) first derivative Ga K edge—Ga metal (dark gray), $PdGa@SiO_2$ (blue), $Ga@SiO_2$ (green), and β-Ga_2O_3 (light gray); (c) Pd K edge—Pd foil (dark gray), $PdGa@SiO_2$ (blue), $Pd@SiO_2$ (red), and PdO (light gray); and Pd K edge EXAFS fits (d) $PdGa@SiO_2$ and (e) $Pd@SiO_2$ (k-weight: 3, fit in light gray).

ing Information S5) shows signals at 126, 94, 30, 27, and 11 ppm, which is consistent with the spectrum of the molecular precursor. The signals at 126 and 94 ppm are assigned to C-sp^2 carbons of COD lying *trans*- to Me and OSi≡ , respectively.[31] The peak at 11 ppm is assigned to Pd-*Me*, which is consistent with a displacement of the large $(t\text{BuO})_3\text{SiO}-$ ligand by a surface siloxy ligand upon grafting. Reduction under a flow of H_2 (1 bar) at 500 °C yields Pd nanoparticles with a size of 1.6 ± 0.4 nm, as shown by TEM, while IR reveals the re-emergence of the isolated silanol band, alongside the disappearance of all bands associated with organic ligands (Supporting Information S5). H_2 and CO chemisorption show an uptake of 0.91 mol_{H2} mol_{Pd}^{-1} and 0.61 mol_{CO} mol_{Pd}^{-1}, respectively (Table 1, Supporting Information S6). Considering a 1:1 CO/Pd stoichiometry,[32] the dispersion from CO chemisorption ($Đ_{CO}$) equals 61%, in a reasonable agreement with the dispersion from TEM ($Đ_{TEM} \approx 70\%$; Supporting Information S9).[32] While H_2 chemisorption is not effective for a determination of the metal dispersion of Pd nanoparticles due to the formation of a stable bulk hydride with larger particles (>2.6 nm),[32] a comparison of the H_2 uptake and $Đ_{CO}$ would correspond to approximately three hydrogen atoms per surface Pd.

With these encouraging results in hand, the molecular precursor (**1**) was next grafted on $Ga@SiO_2$ (Figure 1a), a surface-doped silica prepared via SOMC that contains 0.8 Ga nm^{-2}, to generate a grafted material, $Pd(COD)Me@Ga@SiO_2$. In this case, 1.9 equiv of isobutene per Pd (quantified by NMR, Supporting Information S4) was evolved during grafting. The formation of isobutene in place of $HOSi(OtBu)_3$ is consistent with the presence of Lewis acid sites, which catalyze the decomposition of $HOSi(OtBu)_3$.[29] An IR analysis of the grafted material reveals the emergence of C−H stretching and bending bands, alongside a decreased intensity for the isolated ≡SiOH band (Supporting Information S5), indicative of grafting through the silanol groups. The elemental analysis of the grafted material indicates the presence of 11 equiv of C and 25 equiv of H per Pd, in agreement with the proposed structure (Supporting Information S4). Furthermore, the ^{13}C CP-MAS NMR shows signals at 126, 95, 29, 20, and 11 ppm (Supporting Information S5), consistent with a chemical environment akin to that of the molecular precursor and the surface species grafted on silica; that is, the chemical shift of the olefinic protons and carbons confirms that all surface species are Pd^{II} with a methyl and a siloxy ligand. Treatment under a flow of H_2 (1 bar) at 500 °C yields nanoparticles with a size of 1.6 ± 0.3 nm, as shown by TEM (Figure 1b), while H_2 and CO chemisorption show an uptake of 0.56 mol_{H2} mol_{Pd}^{-1} and 0.55 mol_{CO} mol_{Pd}^{-1} ($Đ_{CO}$ = 55%, Table 1, Supporting Information S6). The H_2 uptake, which corresponds to two H per surface Pd, is significantly lower than the three H per surface Pd than that observed for $Pd@SiO_2$, despite the near-identical particle size according to TEM, and suggests a different electronic structure of Pd in the presence of Ga. Furthermore, the transmission IR of a self-supporting pellet of $PdGa@SiO_2$ exposed to a pressure of CO (10 mbar) at room temperature reveals a strong vibrational band at 2086 cm^{-1} and a much weaker band at 1960 cm^{-1}, assigned to a terminally bound CO on Pd (μ_1-CO_{Pd}) and bridged CO species (μ_2-CO_{Pd}), respectively (Figure 1c, Supporting Information S7). This observation contrasts with what is observed for $Pd@SiO_2$, where two bands of similar intensity at 2094 and 1967 cm^{-1} are attributed to terminal and bridging species,[16,33] and is consistent with the formation of a PdGa alloy, where the presence of a bridging CO species is suppressed through a dilution of surface Pd species.[34] This disparity highlights the intrinsic difference in the interaction of the particles with CO, which can be explained by the dilution of surface Pd by Ga^0 centers. Furthermore, the red-shifted terminal CO bands (ca. 8 cm^{-1}) observed for the bimetallic system provides further evidence for alloying.[34,35]

To gain a greater understanding of the structure of the as-synthesized materials, XAS was performed. For $PdGa@SiO_2$, Ga K edge X-ray absorption near edge structure (XANES) shows two edge features (identified by the two maxima of the first derivative at 10367.5 and 10371.8 eV, Figure 2a,b, Supporting Information S8), indicating the presence of two distinct species—one metallic, at an energy typical for Ga(0), and one Ga^{III} with an edge energy typical of tetracoordinate Ga sites.[36] The absence of any species with the energy expected for octahedral Ga sites indicates that the material formed does not correspond to bulk Ga_2O_3—an observation that contrasts with materials prepared using impregnation techniques.[13,14] The linear combination fit (LCF) of the XANES indicates a ratio of 67:33 for the two species (metallic/oxidic, Supporting Information S8). This ratio is consistent with the formation of

https://doi.org/10.1021/jacsau.1c00021
JACS Au 2021, 1, 450−458

a Ga-rich alloyed phase. The corresponding Pd K edge XANES (Figure 2c, Supporting Information S8) shows a strong shift to lower energy for PdGa@SiO_2 (24 348.1 eV) from that of bulk Pd (24 350.0 eV), while a smaller shift is observed for Pd@SiO_2 (24 348.8 eV), consistent with earlier literature describing the edge energy of supported Pd nanoparticles.[32]

An in situ study of the reduction process, by XAS-TPR (temperature-programmed reduction (H_2)) at the Pd K edge, in combination with an MCR analysis, indicates that Pd^{II} in Pd(COD)Me@Ga@SiO_2 is reduced to Pd^0 under a flow of H_2 at room temperature (Supporting Information S8, Figures S27−S30), highlighting the facile reduction of the molecular precursor employed. Conversely, Ga is gradually reduced and intercalated into palladium nanoparticles as temperature is increased (vide infra), as evidenced by a continuous measurement of both the Ga K and Pd K edges (see Supporting Information S8, Figures S31−S39). Ga K edge XANES (Figures S35−S36) indicates that the formation of a metallic Ga species occurs, while MCR analysis indicates that this is a gradual process (Figure S37). MCR analysis of the corresponding Pd K edge XANES, measured in identical conditions, demonstrates that changes occur simultaneously for Pd (Figure S33), indicating that the reduction and intercalation of Ga occur in unison (see the Supporting Information S8 for an extended discussion).

An analysis of the extended X-ray absorption fine structure (EXAFS) region was also performed. PdGa@SiO_2 was fitted with Pd−Ga scattering path (N = 2.8 ± 0.9, R = 2.48 ± 0.02 Å) and Pd−Pd path (N = 3.1 ± 0.9, R = 2.73 ± 0.01 Å), providing further evidence for the formation of an alloy with 1:1 Pd/Ga stoichiometry (Figure 2d, Supporting Information S8). For comparison, the Pd K edge EXAFS for Pd@SiO_2 was fitted with a Pd−Pd scattering path (Figure 2e, N = 8.1 ± 0.4, R = 2.73 ± 0.002 Å).

The emergence of a feature consistent with Ga^0 in the Ga K edge XANES as well as EXAFS fitting at the Pd K edge indicate that an alloy forms upon reduction under H_2. Furthermore, STEM-EDX mapping indicates the coexistence of Pd and Ga in the nanoparticles, in agreement with the observed configuration from XAS (Supporting Information S9). Overall, the CO adsorption IR, XAS, and EDX show that intimate domains of Pd and Ga, in the form of a PdGa alloy, are present upon reduction of the grafted material at 500 °C.

Catalytic Performance

The catalytic performance of PdGa@SiO_2 and Pd@SiO_2 was then evaluated in the hydrogenation of CO_2 to CH_3OH (3:1:1 H_2/CO_2/Ar, 25 bar, 230 °C) (Figure 3, Table 2, Supporting Information S10). For PdGa@SiO_2, an intrinsic rate of 6.40 $mol_{MeOH+DME}$ mol_{Pd}^{-1} s^{-1} was observed, while Pd@SiO_2 displays a much lower intrinsic rate for CH_3OH (0.14 mmol mol_{Pd}^{-1} s^{-1}). Under the same conditions, Ga@SiO_2 is inactive. The catalyst slowly deactivates (25%) over 36 h on stream. Note also that the CH_3OH formation rate is ca. 1 order of magnitude greater for PdGa@SiO_2 than for Cu-based reference catalysts (Table 2).[11,27] In addition to an increased rate, the PdGa@SiO_2 system displays a significantly increased CH_3OH selectivity (81% vs 20% for Pd@SiO_2). The large difference in selectivity and activity between PdGa@SiO_2 and the parent monometallic materials highlights the remarkable synergistic effect of Pd and Ga. In addition, the high CH_3OH selectivity with PdGa@SiO_2 does not decrease markedly as conversion increases (ca. 75% selective for methanol at 4% conversion, Figure 3), in contrast to Cu/ZrO_2 or Cu/ZnO/Al_2O_3, where a significant drop in selectivity is observed as conversion increases (Table S7).[5] This increased CH_3OH selectivity at higher conversion was already observed in the related Cu−Ga@SiO_2 system (~90%) prepared via SOMC, though the latter shows ca. 1 order of magnitude lower CH_3OH formation rates (0.72 mol_{MeOH} mol_{Cu}^{-1} s^{-1}).[27]

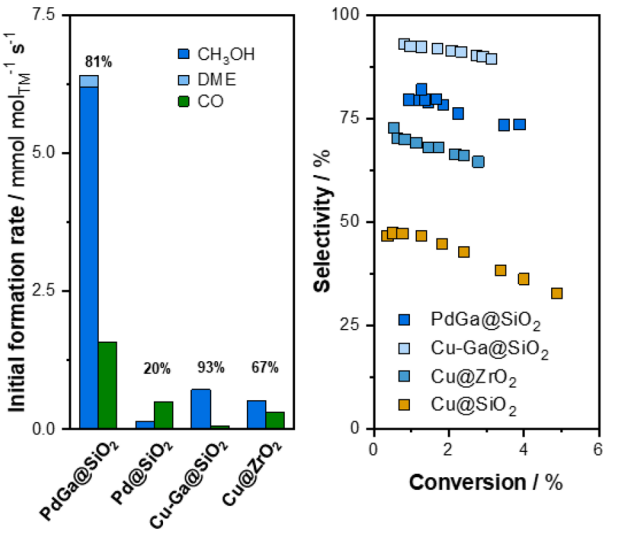

Figure 3. (left) Formation rates for PdGa@SiO_2, Pd@SiO_2, Cu−Ga@SiO_2, and Cu@ZrO_2. (right) Selectivity as a function of conversion for PdGa@SiO_2, Cu−Ga@SiO_2, Cu@SiO_2, Cu@ZrO_2. Conditions: 3:1:1 H_2/CO_2/Ar, 25 bar, 230 °C, 200 mg of catalyst, 5 g of SiC, 6−100 sccm.

Table 2. Summary of Formation Rates and Selectivities for Materials Investigated, Alongside Reference Data for Materials Previously Tested in the Same Conditions

material , (wt% Pd/Cu)	formation rate, mmol s^{-1} $mol_{Pd/Cu}^{-1}$			selectivity
	CH_3OH + DME[a]	CO	CH_4	$S(CH_3OH+DME)$/ $S(CO)$/ $S(CH_4)$
PdGa@SiO_2 (1.08)	6.40	1.57	<0.01[b]	81/19/n/a
Pd@SiO_2 (1.61)	0.14	0.50	0.03	20/75/5
Ga@SiO_2 (n/a)	n/a[b]	n/a[b]	n/a[b]	n/a
Cu@SiO_2[c] (4.5)	0.23	0.24	<0.01[b]	49/51/n/a
Cu@ZrO_2[c] (2.33)	0.51	0.30	n/a	67/33/n/a
CuGa@SiO_2[c] (3.88)	0.72	0.06	n/a	93/7/n/a

[a]Conditions: 3:1:1 (H_2/CO_2/Ar), 25 bar, 230 °C, 200 mg of catalyst, 5 g of SiC, 6−100 sccm. Normalized by mole carbon. n/a indicates not applicable. [b]Below the detection limit of the thermal conductivity detector/flame ionization detector. [c]Previously reported under the same conditions.[11,27]

In Situ and Postreaction Catalyst States

To assess changes to PdGa@SiO_2 under reaction conditions, the material was first analyzed after the reaction. The TEM of PdGa@SiO_2 after the reaction reveals that the particle size does not change after the reaction (1.6 ± 0.4 nm, Figure S11), indicating that the as-synthesized material does not sinter significantly under reaction conditions. Similarly, the XANES of the spent catalyst (PdGa@SiO_2) indicates no significant

https://doi.org/10.1021/jacsau.1c00021
JACS Au 2021, 1, 450−458

changes in the edge energy or the white line intensity for the Pd K edge (24 348.0 eV vs 24 348.1 eV), while the Ga K edge XANES reveals the presence of both a metallic component and a Ga^{III} component (10 367.2 and 10 371.5 eV, Supporting Information S11). The LCF of the Ga K edge gives a Ga^0/Ga^{III} ratio of 46:54, suggesting that part of the alloyed gallium is oxidized under reaction conditions. Notably, the oxidized Ga appears to be exclusively tetracoordinated Ga (Supporting Information S8 and S11). The absence of octahedral Ga sites, typical of Ga_2O_3, is consistent with the formation of highly dispersed Ga sites or small GaO_x clusters upon the segregation of Pd and Ga from the alloy present in the as-synthesized material. The absence of bulk Ga_2O_3 is also consistent with the low formation rate and selectivity for CO, which can readily occur on Ga_2O_3 via RWGS.[30] A study of the material, by Ga K edge XANES under a flow of H_2/CO_2 (5 bar, 230 °C), demonstrates that the material undergoes a partial oxidation under reaction conditions, which is demonstrated by both the increase in the white line intensity and the partial disappearance of the feature at 10 367.5 eV (Supporting Information S11 Figures S54 and S55). The change is, however, reversible; under H_2 at 230 °C, a partial rereduction of a proportion of tetracoordinate Ga is observed, as evidenced by the re-emergence of the feature at 10 367.5 eV (Supporting Information S11 Figures S56 and S57), highlighting the dynamic nature of the dealloying/realloying process for this material.

Study of Bound Surface Adsorbates and Reaction Intermediates

To further understand the divergent reactivity of the mono- and bimetallic systems, the nature of surface adsorbates was probed by IR and NMR spectroscopy. $PdGa@SiO_2$ and $Pd@SiO_2$ were contacted with a H_2/CO_2 mixture (3:1) at 230 °C for 12 h in a high-pressure glass reactor at 5 bar. When cooled, volatiles were removed under reduced pressure, and the solid was analyzed by transmission IR (Figure 4). Analysis of the IR spectrum of the exposed $PdGa@SiO_2$ shows the emergence of peaks at 2996, 2959, 2857, and 1466 cm^{-1}, assigned to surface methoxy species (Supporting Information S12). $PdGa@SiO_2$ was also contacted with a $H_2/^{13}CO_2$ mixture (3:1) at 230 °C for 12 h in a high-pressure glass reactor at 5 bar. ^{13}C CP-MAS, ^1H MAS, and $^1H-^{13}C$ heteronuclear correlation (HETCOR) spectra of the exposed $PdGa@SiO_2$ show signals at 49 ppm (^{13}C) and 3.6 ppm (^1H), consistent with the presence of surface methoxy groups (Supporting Information S12). In contrast, IR spectroscopy on $Pd@SiO_2$ after treatment with H_2/CO_2 at 230 °C and 5 bar shows exclusively peaks at 2091 and 1964 cm^{-1}, assigned to linear and bridged CO species (vide supra, Figure 1c), suggesting that strongly bound carbonyl species may suppress the formation of CH_3OH on $Pd@SiO_2$. In the corresponding experiment using $H_2/^{13}CO_2$, only a very weak signal was observed in the CP-MAS spectrum at 49 ppm (Supporting Information S12), indicating a very low concentration of surface methoxy groups.

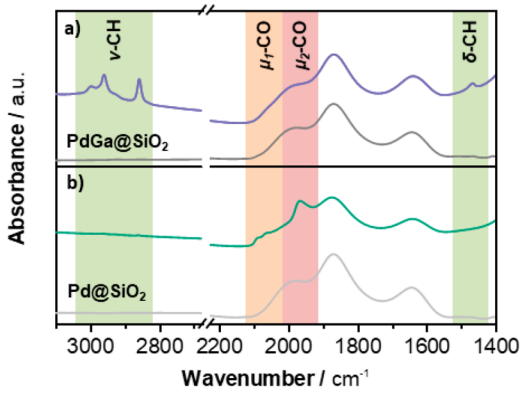

Figure 4. IR analysis after exposure to CO_2/H_2 (3:1) at 230 °C and 5 bar for (a) $PdGa@SiO_2$ exposed (purple, top) and prior to exposure to reaction gases (gray, bottom); (b) $Pd@SiO_2$ exposed (green, top) and prior to exposure to reaction gases (gray, bottom). Reaction time: 12 h.

To have a better understanding of the reaction intermediates at play under reaction conditions, operando DRIFTS on the $PdGa@SiO_2$ catalyst was performed. Under a flow of H_2/CO_2 (3:1) at 20 bar and 230 °C, at steady-state, bands assigned to C−H stretching modes at 2960, 2920, and 2860 cm^{-1} are observed (Figure 5a). The intense bands at 2960 and 2860 cm^{-1} are assigned to methoxy species, while the weak band at 2920 cm^{-1} is assigned to bidentate formate species, consistent with earlier literature.[19] Note that a second peak typically observed for bound formate species, at ∼2860 cm^{-1}, is obscured by the dominant methoxy band (vide infra). Between 2200 and 1200 cm^{-1} (Figure 5b), three kinetically distinct bands are observed, with maxima at 2085, 1920, and 1588 cm^{-1}, which are assigned to terminal CO bound to Pd (μ_1-CO_{Pd}), bridging CO species bound to Pd (μ_n-CO_{Pd}), and the OCO asymmetric stretch of formate species bound to metallic sites, respectively.[37] In contrast to observations from ex situ experiments, both surface carbonyl species and formate species are observed in reaction conditions. Consistent with observations from ex situ experiments, methoxy species are the dominant surface oxygenate species.

To probe the relevance of the observed surface species, we then turned to transient experiments (Figure 5c,d). MCR analysis of switching experiments, between CO_2/He (1:3) and H_2/He (3:1) at 20 bar and 230 °C, reveals three distinct species in the C−H stretching region, assigned to formate and two kinetically distinguishable methoxy species. In addition, the evolution of the bound terminal carbonyl species is observed. In CO_2/He, a rapid buildup of methoxy and terminally bound carbonyl species is observed, alongside a drop in the relative concentration of formate species. When switched to H_2/He, the concentration of methoxy species and carbonyl species falls rapidly, while the concentration of formate increases, with a concomitant increase in methanol formation (Supporting Information S13). These data support that the formation of methanol from methoxy surface species likely involves H_2. In sum, both methoxy and carbonyl species are preferentially stabilized at the catalyst surface under CO_2-rich conditions, while a greater fraction of bound formate species are observed in H_2-rich conditions. The observation that surface formate concentrations are inversely correlated with the concentrations of methoxy and carbonyl species highlights the facile interchange between the two species and the dynamic nature of this catalyst.

Proposed Role of Ga and Implications for Mechanism

Both DRIFTS and XAS indicate that $PdGa@SiO_2$ is a dynamic catalytic system, where the chemical state of Ga and the observed surface intermediates are highly dependent on the chemical potential of the gas phase. Under H_2-rich conditions, an increased proportion of Ga^0 is observed by XAS, with a

https://doi.org/10.1021/jacsau.1c00021
JACS Au 2021, 1, 450−458

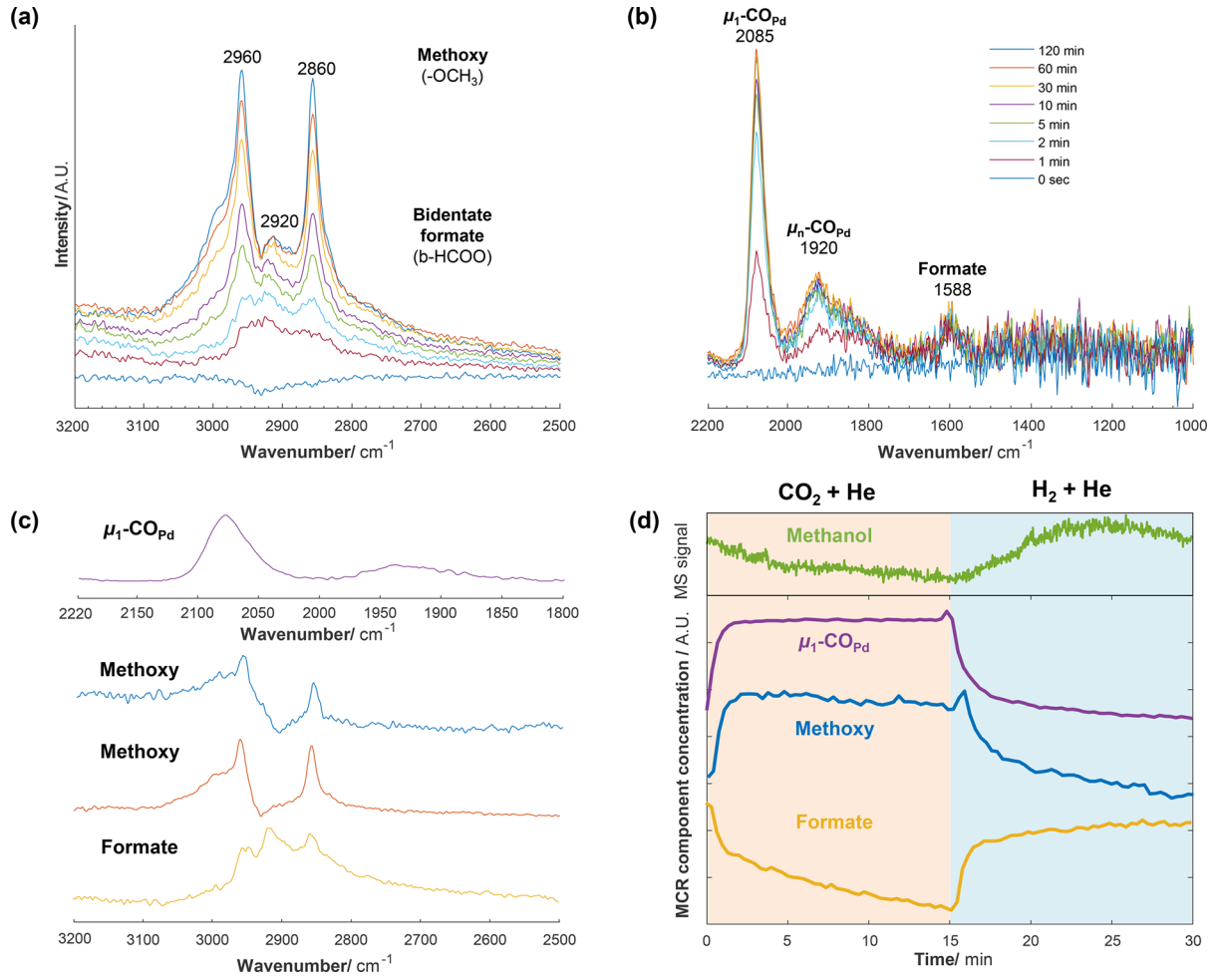

Figure 5. Operando DRIFTS spectra for (a, b) PdGa@SiO_2 under H_2/CO_2 at steady state (3:1, 20 bar, 230 °C); (c) MCR-resolved component profiles, and (d) MCR-resolved concentrations for PdGa@SiO_2 under both CO_2/He (1:3) and H_2/He (3:1). Conditions: 20 bar, 230 °C.

concomitant emergence of formate species according to IR, which could indicate that formate surface species are preferentially stabilized by metallic sites, as previously proposed in the literature.[38] In contrast, under CO_2-rich conditions, an increased proportion of tetracoordinate Ga^{III} is observed, alongside an increase in surface methoxy species, which are most likely stabilized by the Ga^{III} species. This change of preponderant surface intermediates as a function of chemical potential, the low abundance (and stability) of formate species, and the high methanol selectivity at high conversion for this PdGa@SiO_2 catalyst contrasts what is observed for Cu/ZrO_2 and related materials, where formates are invariably observed as stable surface adsorbates and methanol selectivity deteriorates with increasing conversion. Furthermore, it has been shown that the over stabilization of formate intermediates, clearly observed for Cu/Al_2O_3, leads to the formation of methyl formate with increasing CO_2 conversion (high methanol concentrations), which has been shown to decompose into methanol and CO under these conditions, thus decreasing the methanol selectivity.[39] Hence, the lower stability of formate intermediates is likely linked to the higher observed methanol selectivity at an elevated conversion for PdGa@SiO_2 catalysts. These results support that an efficient methanol synthesis from CO_2 should involve a fast conversion of CO_2 to formate, formate to methoxy intermediates, before formation and desorption of methanol. Overall, the results discussed above could indicate that the ease of alloying-dealloying combined with the correlation between this phenomenon and the detection/stabilization of formate intermediates that the efficient alloying-dealloying process in this highly dynamic PdGa catalyst could be at the origin of its improved methanol activity and selectivity at higher CO_2 conversion, since it would avoid an accumulation of formate intermediates and increase the rate of methanol formation.

CONCLUSIONS

In summary, PdGa@SiO_2, prepared via SOMC using a tailored traceless Pd molecular precursor and a Ga-doped silica surface, is a highly selective and active catalyst for the hydrogenation of CO_2 to CH_3OH, displaying activity an order of magnitude greater than the benchmark Cu-based systems. In contrast to previously reported Pd-based systems, the CH_3OH selectivity is high (ca. 80%), and it does not decrease markedly at a higher conversion, suggesting that the use of a gallium-doped silica support containing exclusively isolated Ga^{III} sites prevents the formation of larger Ga_2O_3 domains, which are known to promote RWGS. Analysis of the reduction process by XAS-TPR indicates that the PdGa alloy is formed through a gradual intercalation of Ga to Pd nanoparticles at elevated temperatures.

A study of the material under reaction conditions reveals that, while partial oxidation of Ga^0 occurs, the Ga^{III} species are

https://doi.org/10.1021/jacsau.1c00021
JACS Au 2021, 1, 450−458

exclusively tetracoordinate Ga sites. IR and NMR experiments allow the detection of surface-stabilized methoxy groups on $PdGa@SiO_2$. An in situ study of $PdGa@SiO_2$, by XAS, indicates that there are facile redox processes enabling the transformation between Ga^0/Ga^{III} under CO_2 hydrogenation conditions, while the observed reaction intermediates, probed by operando DRIFTS, show a similar dependence on the gas-phase composition. Transient experiments reveal the presence of both methoxy and formate species under reaction conditions, with the two surface species having inversely proportional concentrations. These observations highlight the subtle role of dynamic dealloying/realloying processes and how this can be exploited to generate highly active and selective catalytic systems. Further studies into the subtle interplay between the Pd/Ga and $Pd/Ga^{III}O_x$ are currently underway, with the goal to understand the origin of the observed synergistic behavior between Pd and Ga; other research efforts are directed at exploring the general applicability of this approach toward the formation of oxide-supported PdM nanoparticles and their application in selective hydrogenation reactions.

EXPERIMENTAL SECTION

Synthesis of Pd(COD)Me(OSi(O*t*Bu)$_3$)

Pd(COD)MeCl (1.00 g, 3.77 mmol) was dissolved in toluene (80 mL). To this was added a solution of $NaOSi(OtBu)_3$ (1.08 g, 3.77 mmol) in toluene (20 mL), followed by successive washings of the reaction vessel (2 × 10 mL). The reaction mixture was stirred, at room temperature, for 16 h. The solvent was removed under reduced pressure to yield a dark solid. The remaining solid was washed with Et_2O (3 × 10 mL), and the combined washings were concentrated under reduced pressure to yield a white crystalline solid. The solid was dissolved in CH_2Cl_2 (10 mL) and cooled to −40 °C to yield a small amount of white crystals. The reaction mixture was filtered over diatomaceous earth, and the supernatant was collected and concentrated under reduced pressure to yield a yellow solid. The solid was dissolved in pentane (3 mL) and cooled to −40 °C overnight, to yield colorless rhombohedral crystals. Successive recrystallizations yielded 1.16 g of product (62% yield).

Synthesis of Pd(COD)Me@Ga@SiO_{2-700}

To a suspension of $Ga@SiO_2$ (1.000 g) in C_6H_6 (20 mL) was added a clear solution of Pd(COD)Me(OSi(O*t*Bu)$_3$) (78.9 mg, 0.16 mmol) in C_6H_6 (10 mL). The suspension was stirred for 1 h at 25 °C. After it was stirred, the material was filtered, rinsed with C_6H_6 (3 × 7 mL), and dried under under high vacuum (10^{-5} mbar). Isobutene (1.9 equiv) was identified as the side product of the reaction.

Synthesis of $PdGa@SiO_{2-700}$

To a glass flow reactor containing a medium porosity glass frit was added $Pd(COD)Me@Ga@SiO_2$ (0.773 g). The flow reactor was evacuated (10^{-5} mbar) and then filled with H_2. The reactor was subsequently heated to 500 °C (5 °C min^{-1}) while maintaining a flow of H_2 (960 mbar(a)). After 12 h of heating, the reactor was evacuated (10^{-5} mbar), while still hot, yielding a dark solid material.

General Considerations

Unless otherwise indicated, all manipulations were undertaken using conventional air-free techniques (argon). All solvents were purified by a solvent purification system (SPS) or by drying followed by distillation and stored over activated molecular sieves. [Mg-$(CH_2Ph)_2(THF)_2$], $Pd(COD)Cl_2$, $Ga(OSi(OtBu)_3)_3(THF)$, and $HOSi(OtBu)_3$ (THF = tetrahydrofuran) were synthesized as described in earlier literature.[29,40−42] Silica (Aerosil Degussa, 200 $m^2\ g^{-1}$) was compacted with deionized water, dried at 100 °C for 7 d, crushed, and sieved (250−400 μm) for easier handling. Silica-700 (SiO_{2-700}) was calcined at 500 °C in air for 12 h, allowed to return to room temperature, and treated under high vacuum (10^{-5} mbar) at 500 °C for 12 h (ramp: 5 °C min^{-1}) and then at 700 °C for 24 h (ramp: 1.7 °C min^{-1}).

Attenuated total reflectance (ATR) IR spectra were recorded inside an Ar-filled glovebox on a Bruker FT-IR Alpha spectrometer. Transmission-IR were recorded on Bruker FT-IR Alpha spectrometer or a Nicolet 6700 FTIR spectrophotometer. Spectra are normalized to the Si−O−Si overtone peak maximum at 1868 cm^{-1} for all materials. Solution NMR spectra were obtained on BrukerR DRX 300 spectrometer (7.05 T, Larmor Frequency: 300 MHz (^{1}H), 75.5 MHz (^{13}C)). ^{1}H and ^{13}C chemical shifts are referenced relative to residual solvent peaks.[43] Solid-state NMR spectra of grafted samples were recorded on a Bruker 400 MHz NMR spectrometer using a double-resonance 4 or 3.2 mm probe. Single-crystal XRD was performed on a Bruker APEX-II CCD diffractometer, and structures were solved with the olex2.solve structure solution program[44] using Charge Flipping and refined with the ShelXL[45] refinement package using Least Squares minimization. Particle size estimations were obtained by transmission electron microscopy (JEOL JEM-1400 Plus microscope). Energy-dispersive X-ray mapping was measured on a Talos F200 X microscope. XAS measurements were performed at the Pd and Ga K edges at the SuperXAS beamline at SLS (PSI). The program package Demeter was used for the analysis of EXAFS.[46] For operando DRIFTS experiments, a custom-made high-pressure reaction cell was mounted in a Harrick Praying Mantis diffuse reflection (DRIFTS) accessory. The spectra were collected using a Thermo Scientific Nicolet 6700 FT-IR spectrometer. The outlet gas stream was analyzed by a Pfeiffer OmniStar GSD 300C mass spectrometer.

CO_2 hydrogenation rates were measured at 230 °C at differential conversions (<10%) on all samples. Samples were loaded in an argon-filled glovebox. Samples were treated at 300 °C in 5:1 H_2/N_2 (60 sccm, 1 bar) for 1 h before being cooled to the reaction temperature (230 °C in N_2 flow (50 sccm, 1 bar)), after which, CO_2, H_2, and Ar (1:3:1) were introduced, and the reactor was pressurized (25 bar). The reactor pressure was maintained by a back-pressure regulator (Bronkhorst EL-PRESS). Gas flow rates were screened in the range from 100 to 6 sccm. Reactant and product concentrations in the reactant and effluent streams were measured by online gas chromatography (Agilent 7890N GC). Product selectivity is defined on a per-carbon basis. Intrinsic formation rates (i.e., rate at zero contact time) are obtained by using a second-order polynomial fit on the experimental data and extrapolating to zero residence time.

Experimental procedures, purification procedures for commercial chemicals, instrument specifications, and characterization data are covered in greater detail in the Supporting Information.

ASSOCIATED CONTENT

Supporting Information

The Supporting Information is available free of charge at https://pubs.acs.org/doi/10.1021/jacsau.1c00021.

Complete experimental procedures, general considerations, spectroscopic methods, and associated data (PDF)

Crystallographic data file for **1** (CCDC Deposition No. 2007107) (CIF)

AUTHOR INFORMATION

Corresponding Author

Christophe Copéret − *Department of Chemistry and Applied Biosciences, ETH Zürich, CH-8093 Zurich, Switzerland;* orcid.org/0000-0001-9660-3890; Email: ccoperet@ethz.ch

https://doi.org/10.1021/jacsau.1c00021
JACS Au 2021, 1, 450−458

Authors

Scott R. Docherty − *Department of Chemistry and Applied Biosciences, ETH Zürich, CH-8093 Zurich, Switzerland;* orcid.org/0000-0002-8605-3669

Nat Phongprueksathat − *Catalysis Engineering, Department of Chemical Engineering, Delft University of Technology, 2629 HZ Delft, The Netherlands;* orcid.org/0000-0003-4225-8205

Erwin Lam − *Department of Chemistry and Applied Biosciences, ETH Zürich, CH-8093 Zurich, Switzerland*

Gina Noh − *Department of Chemistry and Applied Biosciences, ETH Zürich, CH-8093 Zurich, Switzerland;* orcid.org/0000-0003-4717-5767

Olga V. Safonova − *Paul Scherrer Institute, CH-5232 Villigen, Switzerland;* orcid.org/0000-0002-6772-1414

Atsushi Urakawa − *Catalysis Engineering, Department of Chemical Engineering, Delft University of Technology, 2629 HZ Delft, The Netherlands;* orcid.org/0000-0001-7778-4008

Complete contact information is available at: https://pubs.acs.org/10.1021/jacsau.1c00021

Author Contributions

All authors have given approval to the final version of the manuscript.

Notes

The authors declare no competing financial interest.

■ ACKNOWLEDGMENTS

S.D., N.P., O.V.S., A.U., and C.C.H. thank the Swiss National Science Foundation (Grant Nos. 200021_169134 and CRSII5_183495) for funding. Part of this research was also funded by the SCCER Heat and Energy Storage program (InnoSuisse). The authors acknowledge J. Alfke, C. P. Gordon, and D. Trummer for assistance with XAS, SS-NMR, and X-ray crystallography, respectively. The authors thank L. Rochlitz and Dr X. Huang for recording TEM carried out at ScopeM. The authors also thank PSI SuperXAS for beamtime and provision of Ga^0 and Pd^0 reference materials.

■ REFERENCES

(1) Kondratenko, E. V.; Mul, G.; Baltrusaitis, J.; Larrazábal, G. O.; Pérez-Ramírez, J. Status and Perspectives of CO_2 Conversion into Fuels and Chemicals by Catalytic, Photocatalytic and Electrocatalytic Processes. *Energy Environ. Sci.* **2013**, *6* (11), 3112−3135.

(2) Goeppert, A.; Czaun, M.; Jones, J.-P.; Surya Prakash, G. K.; Olah, G. A. Recycling of Carbon Dioxide to Methanol and Derived Products − Closing the Loop. *Chem. Soc. Rev.* **2014**, *43* (23), 7995−8048.

(3) Olah, G. A. Towards Oil Independence Through Renewable Methanol Chemistry. *Angew. Chem., Int. Ed.* **2013**, *52* (1), 104−107.

(4) Álvarez, A.; Bansode, A.; Urakawa, A.; Bavykina, A. V.; Wezendonk, T. A.; Makkee, M.; Gascon, J.; Kapteijn, F. Challenges in the Greener Production of Formates/Formic Acid, Methanol, and DME by Heterogeneously Catalyzed CO_2 Hydrogenation Processes. *Chem. Rev.* **2017**, *117* (14), 9804−9838.

(5) Jiang, X.; Nie, X.; Guo, X.; Song, C.; Chen, J. G. Recent Advances in Carbon Dioxide Hydrogenation to Methanol via Heterogeneous Catalysis. *Chem. Rev.* **2020**, *120* (15), 7984−8034.

(6) Kasatkin, I.; Kurr, P.; Kniep, B.; Trunschke, A.; Schlögl, R. Role of Lattice Strain and Defects in Copper Particles on the Activity of $Cu/ZnO/Al_2O_3$ Catalysts for Methanol Synthesis. *Angew. Chem., Int. Ed.* **2007**, *46* (38), 7324−7327.

(7) Chinchen, G. C.; Denny, P. J.; Jennings, J. R.; Spencer, M. S.; Waugh, K. C. Synthesis of Methanol: Part 1. Catalysts and Kinetics. *Appl. Catal.* **1988**, *36*, 1−65.

(8) Bart, J. C. J.; Sneeden, R. P. A. Copper-Zinc Oxide-Alumina Methanol Catalysts Revisited. *Catal. Today* **1987**, *2* (1), 1−124.

(9) Schild, C.; Wokaun, A.; Baiker, A. On the Hydrogenation of CO and CO_2 over Copper/Zirconia and Palladium/Zirconia Catalysts. *Fresenius' J. Anal. Chem.* **1991**, *341* (5), 395−401.

(10) Fisher, I. A.; Woo, H. C.; Bell, A. T. Effects of Zirconia Promotion on the Activity of Cu/SiO_2 for Methanol Synthesis from CO/H_2 and CO_2/H_2. *Catal. Lett.* **1997**, *44* (1), 11−17.

(11) Larmier, K.; Liao, W.-C.; Tada, S.; Lam, E.; Verel, R.; Bansode, A.; Urakawa, A.; Comas-Vives, A.; Copéret, C. CO_2-to-Methanol Hydrogenation on Zirconia-Supported Copper Nanoparticles: Reaction Intermediates and the Role of the Metal−Support Interface. *Angew. Chem., Int. Ed.* **2017**, *56* (9), 2318−2323.

(12) Sahibzada, M.; Metcalfe, I. S.; Chadwick, D. Methanol Synthesis from $CO/CO_2/H_2$ over $Cu/ZnO/Al_2O_3$ at Differential and Finite Conversions. *J. Catal.* **1998**, *174* (2), 111−118.

(13) Collins, S. E.; Baltanás, M. A.; Bonivardi, A. L. An Infrared Study of the Intermediates of Methanol Synthesis from Carbon Dioxide over $Pd/\beta\text{-}Ga_2O_3$. *J. Catal.* **2004**, *226*, 410.

(14) Collins, S. E.; Delgado, J. J.; Mira, C.; Calvino, J. J.; Bernal, S.; Chiavassa, D. L.; Baltanás, M. A.; Bonivardi, A. L. The Role of Pd−Ga Bimetallic Particles in the Bifunctional Mechanism of Selective Methanol Synthesis via CO_2 Hydrogenation on a Pd/Ga_2O_3 Catalyst. *J. Catal.* **2012**, *292*, 90−98.

(15) Arana, J.; Homs, N.; Sales, J.; Fierro, J.L.G.; Ramirez de la Piscina, P. CO/CO_2 Hydrogenation and Ethylene Hydroformylation over Silica-Supported PdZn Catalysts. *Catal. Lett.* **2001**, *72* (3), 183−189.

(16) Ota, A.; Kunkes, E. L.; Kasatkin, I.; Groppo, E.; Ferri, D.; Poceiro, B.; Navarro Yerga, R. M.; Behrens, M. Comparative Study of Hydrotalcite-Derived Supported Pd_2Ga and PdZn Intermetallic Nanoparticles as Methanol Synthesis and Methanol Steam Reforming Catalysts. *J. Catal.* **2012**, *293*, 27−38.

(17) Fiordaliso, E. M.; Sharafutdinov, I.; Carvalho, H. W. P.; Grunwaldt, J.-D.; Hansen, T. W.; Chorkendorff, I.; Wagner, J. B.; Damsgaard, C. D. Intermetallic $GaPd_2$ Nanoparticles on SiO_2 for Low-Pressure CO_2 Hydrogenation to Methanol: Catalytic Performance and In Situ Characterization. *ACS Catal.* **2015**, *5* (10), 5827−5836.

(18) Bowker, M. Methanol Synthesis from CO_2 Hydrogenation. *ChemCatChem* **2019**, *11* (17), 4238−4246.

(19) Manrique, R.; Rodríguez-Pereira, J.; Rincón-Ortiz, S. A.; Bravo-Suárez, J. J.; Baldovino-Medrano, V. G.; Jiménez, R.; Karelovic, A. The Nature of the Active Sites of Pd−Ga Catalysts in the Hydrogenation of CO_2 to Methanol. *Catal. Sci. Technol.* **2020**, *10* (19), 6644−6658.

(20) Manrique, R.; Jiménez, R.; Rodríguez-Pereira, J.; Baldovino-Medrano, V. G.; Karelovic, A. Insights into the Role of Zn and Ga in the Hydrogenation of CO_2 to Methanol over Pd. *Int. J. Hydrogen Energy* **2019**, *44* (31), 16526−16536.

(21) Fujitani, T.; Saito, M.; Kanai, Y.; Watanabe, T.; Nakamura, J.; Uchijima, T. Development of an Active Ga_2O_3 Supported Palladium Catalyst for the Synthesis of Methanol from Carbon Dioxide and Hydrogen. *Appl. Catal., A* **1995**, *125* (2), L199−L202.

(22) Oyola-Rivera, O.; Baltanás, M. A.; Cardona-Martínez, N. CO_2 Hydrogenation to Methanol and Dimethyl Ether by $Pd-Pd_2Ga$ Catalysts Supported over Ga_2O_3 Polymorphs. *J. CO_2 Util.* **2015**, *9*, 8−15.

(23) García-Trenco, A.; White, E. R.; Regoutz, A.; Payne, D. J.; Shaffer, M. S. P.; Williams, C. K. Pd_2Ga-Based Colloids as Highly Active Catalysts for the Hydrogenation of CO_2 to Methanol. *ACS Catal.* **2017**, *7* (2), 1186−1196.

(24) Lam, E.; Larmier, K.; Wolf, P.; Tada, S.; Safonova, O. V.; Copéret, C. Isolated Zr Surface Sites on Silica Promote Hydrogenation of CO_2 to CH_3OH in Supported Cu Catalysts. *J. Am. Chem. Soc.* **2018**, *140* (33), 10530−10535.

(25) Noh, G.; Docherty, S. R.; Lam, E.; Huang, X.; Mance, D.; Alfke, J. L.; Copéret, C. CO_2 Hydrogenation to CH_3OH on Supported Cu Nanoparticles: Nature and Role of Ti in Bulk Oxides vs Isolated Surface Sites. *J. Phys. Chem. C* **2019**, *123* (51), 31082−31093.
(26) Noh, G.; Lam, E.; Alfke, J. L.; Larmier, K.; Searles, K.; Wolf, P.; Copéret, C. Selective Hydrogenation of CO_2 to CH_3OH on Supported Cu Nanoparticles Promoted by Isolated Ti^{IV} Surface Sites on SiO_2. *ChemSusChem* **2019**, *12* (5), 968−972.
(27) Lam, E.; Noh, G.; Chan, K. W.; Larmier, K.; Lebedev, D.; Searles, K.; Wolf, P.; Safonova, O. V.; Copéret, C. Enhanced CH_3OH Selectivity in CO_2 Hydrogenation Using Cu-Based Catalysts Generated via SOMC from Ga^{III} Single-Sites. *Chem. Sci.* **2020**, *11*, 7593−7598.
(28) Copéret, C. Single-Sites and Nanoparticles at Tailored Interfaces Prepared via Surface Organometallic Chemistry from Thermolytic Molecular Precursors. *Acc. Chem. Res.* **2019**, *52* (6), 1697−1708.
(29) Searles, K.; Siddiqi, G.; Safonova, O. V.; Copéret, C. Silica-Supported Isolated Gallium Sites as Highly Active, Selective and Stable Propane Dehydrogenation Catalysts. *Chem. Sci.* **2017**, *8* (4), 2661−2666.
(30) Zhao, B.; Pan, Y.; Liu, C. The Promotion Effect of CeO_2 on CO_2 Adsorption and Hydrogenation over Ga_2O_3. *Catal. Today* **2012**, *194* (1), 60−64.
(31) Laurent, P.; Veyre, L.; Thieuleux, C.; Donet, S.; Copéret, C. From Well-Defined Pt(II) Surface Species to the Controlled Growth of Silica Supported Pt Nanoparticles. *Dalt. Trans.* **2013**, *42* (1), 238−248.
(32) Tew, M. W.; Miller, J. T.; van Bokhoven, J. A. Particle Size Effect of Hydride Formation and Surface Hydrogen Adsorption of Nanosized Palladium Catalysts: L_3 Edge vs K Edge X-Ray Absorption Spectroscopy. *J. Phys. Chem. C* **2009**, *113* (34), 15140−15147.
(33) Sheppard, N.; De La Cruz, C. The Reliability of Vibrational Spectroscopy as a Means of Identification of the Structures of Chemisorbed Species on Metal Surfaces: The Cases of CO, NO and C_2 Hydrocarbon Surface Species. *Catal. Today* **2001**, *70* (1−3), 3−13.
(34) Kovnir, K.; Armbrüster, M.; Teschner, D.; Venkov, T. V.; Szentmiklósi, L.; Jentoft, F. C.; Knop-Gericke, A.; Grin, Y.; Schlögl, R. In Situ Surface Characterization of the Intermetallic Compound PdGa − A Highly Selective Hydrogenation Catalyst. *Surf. Sci.* **2009**, *603* (10), 1784−1792.
(35) Su, X.; Lin, W.; Cheng, H.; Zhang, C.; Li, Y.; Liu, T.; Zhang, B.; Wu, Q.; Yu, X.; Zhao, F. PdGa/TiO_2 an Efficient Heterogeneous Catalyst for Direct Methylation of N-Methylaniline with CO_2/H_2. *RSC Adv.* **2016**, *6* (105), 103650−103656.
(36) Nishi, K.; Shimizu, K.; Takamatsu, M.; Yoshida, H.; Satsuma, A.; Tanaka, T.; Yoshida, S.; Hattori, T. Deconvolution Analysis of Ga K-Edge XANES for Quantification of Gallium Coordinations in Oxide Environments. *J. Phys. Chem. B* **1998**, *102* (50), 10190−10195.
(37) Sun, Q.; Chen, B. W. J.; Wang, N.; He, Q.; Chang, A.; Yang, C.-M.; Asakura, H.; Tanaka, T.; Hülsey, M. J.; Wang, C.-H.; Yu, J.; Yan, N. Zeolite-Encaged Pd−Mn Nanocatalysts for CO_2 Hydrogenation and Formic Acid Dehydrogenation. *Angew. Chem., Int. Ed.* **2020**, *59* (45), 20183−20191.
(38) Corral-Pérez, J. J.; Bansode, A.; Praveen, C. S.; Kokalj, A.; Reymond, H.; Comas-Vives, A.; VandeVondele, J.; Copéret, C.; von Rohr, P. R.; Urakawa, A. Decisive Role of Perimeter Sites in Silica-Supported Ag Nanoparticles in Selective Hydrogenation of CO_2 to Methyl Formate in the Presence of Methanol. *J. Am. Chem. Soc.* **2018**, *140* (42), 13884−13891.
(39) Copéret, C.; Lam, E.; Corral-Pérez, J. J.; Larmier, K.; Noh, G.; Wolf, P.; Comas-Vives, A.; Urakawa, A. CO_2 Hydrogenation on Cu/Al_2O_3: Role of Metal/Support Interface in Driving Activity and Selectivity of a Bifunctional Catalyst. *Angew. Chem., Int. Ed.* **2019**, *58* (39), 13989−13996.
(40) Drew, D.; Doyle, J. R.; Shaver, A. G. Cyclic Diolefin Complexes of Platinum and Palladium. In *Inorganic Syntheses;* John Wiley & Sons, Ltd, 2007; pp 47−55. DOI: 10.1002/9780470132449.ch11.
(41) Sandoval, J. J.; Palma, P.; Álvarez, E.; Cámpora, J.; Rodríguez-Delgado, A. Mechanism of Alkyl Migration in Diorganomagnesium 2,6-Bis(Imino)Pyridine Complexes: Formation of Grignard-Type Complexes with Square-Planar Mg(II) Centers. *Organometallics* **2016**, *35* (18), 3197−3204.
(42) Docherty, S. R.; Estes, D. P.; Copéret, C. Facile Synthesis of Unsymmetrical Trialkoxysilanols: $(RO)_2(R'O)SiOH$. *Helv. Chim. Acta* **2018**, *101* (3), e1700298 DOI: 10.1002/hlca.201700298.
(43) Fulmer, G. R.; Miller, A. J. M.; Sherden, N. H.; Gottlieb, H. E.; Nudelman, A.; Stoltz, B. M.; Bercaw, J. E.; Goldberg, K. I. NMR Chemical Shifts of Trace Impurities: Common Laboratory Solvents, Organics, and Gases in Deuterated Solvents Relevant to the Organometallic Chemist. *Organometallics* **2010**, *29* (9), 2176−2179.
(44) Bourhis, L. J.; Dolomanov, O. V.; Gildea, R. J.; Howard, J. A. K.; Puschmann, H. The Anatomy of a Comprehensive Constrained, Restrained Refinement Program for the Modern Computing Environment - Olex2 Dissected. *Acta Crystallogr., Sect. A: Found. Adv.* **2015**, *71* (1), 59−75.
(45) Sheldrick, G. M. Crystal Structure Refinement with SHELXL. *Acta Crystallogr., Sect. C: Struct. Chem.* **2015**, *71* (1), 3−8.
(46) Ravel, B.; Newville, M. ATHENA, ARTEMIS, HEPHAESTUS: Data Analysis for X-Ray Absorption Spectroscopy Using IFEFFIT. *J. Synchrotron Radiat.* **2005**, *12* (4), 537−541.

https://doi.org/10.1021/jacsau.1c00021
JACS Au 2021, 1, 450−458